RSC Advances

ROYAL SOCIETY OF CHEMISTRY

www.rsc.org/advances

A facile route for preparation of monodisperse nanoparticles of one-dimensional Fe(II)-4-amino-1, 2, 4-triazole coordination polymer with hysteretic spin-crossover near room temperature

Meng-Ya Chen,[a] Xuan-Rong Chen,[a] Wei-Hua Ning,[a] Xiao-Ming Ren* [a, b, c]

[a]State Key Laboratory of Material-Oriented Chemical Engineering and College of Science, Nanjing Tech University, Nanjing 210009, P.R. China

[b]College of Materials Science and Engineering, Nanjing Tech University, Nanjing 210009, P.R. China

[c]State Key Laboratory of Coordination Chemistry, Nanjing University, Nanjing 210093, P. R. China

Tel.: +86 25 58139476

Fax: +86 25 58139481

E-mail: xmren@njtech.edu.cn

Abstract

Spin-crossover (SCO) occurred in a transition metal complex is the switchable process between two spin states in response to external perturbations such as changes in temperature, pressure or photoexcitation. Such a material has potential applications in the switching devices. In this study, we designed a one-dimensional spin-crossover polymer, with a formula of $[Fe(NH_2\text{-}Trz)_3](doe)_2$ where NH_2-Trz = 4-amino-1,2,4-triazole and doe = sodium dodecyl sulfonate, and fabricated its monodisperse nanoparticles using a facile precipitation route. The nanoparticles aggregate from plate-shaped nanocrystals and their size dimensions fall in the ranges of 200−300 nm. The SCO polymer undergoes a thermal reversible spin transition near room temperature which is important for the practical applications. The spin transition shows ca. 13 K hysteretic loops and associates with color change. The SCO polymer nanoparticles were pressed under the ca. 8 MPa static pressure to give a good transparent disc with a thickness of ca. 1 mm, such a disc displays pink-violet color at ambient temperature while yellowish color above 45 °C. This SCO material has potential application in the field of thermochromic devices.

Keywords: Spin-crossover polymer, monodisperse nanoparticles, thermochromic phenomenon, hysteretic spin transition

Introduction

Phase transitions in materials occur widely in nature and can often impart functionality to the system, sometimes leading to important technological innovations. The physical properties of a material may change massively across a solid-to-solid phase transition.[1–9] For instance, vanadium dioxide (VO_2), undergoes a metal-to-insulator (MI) transition at 341 K and shows dramatic changes in electrical resistivity and infrared transmission across this phase transition.[10,11] An organic molecular conductor, based on a spiro-biphenalenyl neutral radical, goes through a structural phase transition near room temperature and simultaneously exhibits bistability in electrical, optical and magnetic properties.[8] As a consequence, materials that undergo fast, reversible, and especially hysteretic phase transition is very useful for applications as switching devices.[1, 11]

Spin crossover (SCO) is the switching process between two spin states occurring within octahedrally coordinated transition-metal (TM) ions bearing d^4-d^7 electronic configurations. A variety of external perturbations have been shown to induce the effect, including variations in temperature and pressure, illumination and exposure to magnetic fields.[12-17] These types of materials have recently attracted much research interest because their promising applications are predicated in the development of new information storage and optical[18-22] as well as spintronics[23,24] devices. In order to study the effect of the domain size on the cooperativity of the SCO transition (hysteresis and transition temperature) and thus to use these materials in information storage and other devices, one important goal is to synthesize controlled objects at the nanoscale. To this end, it has recently been demonstrated that monodisperse nanoscale particles of SCO coordination polymers[25-30] can be fabricated by exploiting the established micelle techniques (i.e., the "bottom-up" approach and some surfactants were generally used for preventing nanoparticles aggregation). This is an important step for emerging nanoscale technologies, as the alternate approach for miniaturizing particle size through mechanical processing into smaller particles (i.e., the "top-down" approach) results in gradual, diminished or even nonexistent SCO

characteristics.[30]

From viewpoint of practical application, it is important that the SCO transition temperature is near room temperature. Among numerous SCO compounds, some of the most promising candidates come from the $[Fe(NH_2\text{-}Trz)_3](X)_2$ (NH_2-Trz = 4-amino-1,2,4-triazole and X is counter anion) family.[31-37] In these compounds, the metal ions are bound by the bridging ligands of 4-amino-1,2,4-triazoles, giving one-dimensional (1-D) polymeric structures (Scheme 1)[37] that exhibit a cooperative spin transition between Fe^{2+} low spin (LS) and high spin (HS).

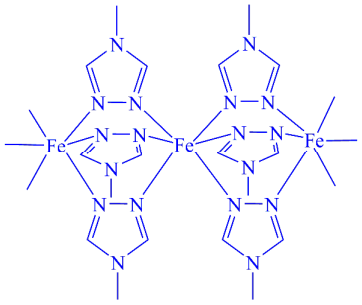

Scheme 1 Illustration for the structure of 1-D coordination polymeric chain in $[Fe(NH_2\text{-}Trz)_3](X)_2$ family[37]

In this study, we designed the SCO coordination polymer $[Fe(NH_2\text{-}Trz)_3](doe)_2$ where doe = sodium dodecyl sulfonate as the object compound because the transition temperature in 1-D polymer $[Fe(NH_2\text{-}Trz)_3](X)_2$ is usually near room temperature and the dodecyl sulfonate can be acted as the surfactant and the counter ions as well. We fabricated the monodisperse SCO nanoparticles with size dimensions of 200-300 nm using a facile precipitation route in surfactant-free condition. Herein we reported the spin-crossover and thermochromic behaviors for the monodisperse SCO nanoparticles.

Experimental section

Chemicals and Materials

All solvents and reagents were obtained from commercial sources as analytical grade and directly used without further purification.

Fabrication nanoparticles of coordination polymer (1)

A 2 mL methanol-water (V/V = 1:1) solution containing $Fe(BF_4)_2 \cdot 6H_2O$ (84 mg, 0.25 mmol) with a small amount of ascorbic acid was added to 5 mL aqueous solution containing sodium dodecyl sulfonate (68 mg, 0.25mol), the mixture was vigorously stirred at ambient temperature to give a solution A. On the other hand, 4-amino-1, 2, 4-triazole (63 mg, 0.75 mmol) and sodium dodecyl sulfonate (68 mg, 0.25mol) were dissolved in 7 mL water to give aqueous solution B. The solutions A and B were mixed with magnetic stirring at room temperature; the purple precipitate gradually formed, which was collected by filtration and washed using methanol. The collected purple precipitate was dried in vacuum at 50 °C for a half hour. Elemental analyses calculated for $FeC_{31}H_{68}N_{12}S_2O_8$: C: 43.45, H: 8.00, N: 19.61. Found: C: 43.23, H: 7.66, N: 19.39.

It is noticeable that the reaction gave white precipitate if the solutions A and B were mixed at the temperature above 50 °C, such a white product did not show spin crossover behavior, as a result, it was not fully characterized.

Physical measurements

Elemental analyses (C, H and N) were performed with an Elementar Vario EL III analyzer. Thermogravimetric (TG) analysis was performed on a SDT Q600 V20.9 Build 20, in the temperature ranges of 293–1023 K (20–750 °C) under nitrogen atmosphere, and the heating rate is 20 K/min. Differential Scanning Calorimetry (DSC) measurement was carried out on a DSC Q2000 V24.10 Build 122 for powder sample in temperature range between 223 K (-50 °C) and 473 K (200 °C), with a temperature scanning rate of 10 K/min. Temperature dependent magnetic susceptibility of **1** was measured using a XS-5 superconducting quantum interference device (SQUID) for powder sample in the temperature range of 1.8-400 K upon heating and cooling cycles and the diamagnetism arisen from contribution of atom core was not removed. Raman spectra were recorded in the backscattering geometry with a Labram HR 800 Raman spectrometer (Horiba Jobin-Yvon) coupled to an Olympus co-focal microscope and equipped with a laser operating at 514 nm. The morphology of powder samples were observed by a Hitachi S4800 field emission

scanning microscope (FESEM) operated at 5 kV. The purple precipitate was ultrasonic distribution in absolute EtOH using a SCIENTZ-IID ultrasonic instrument (Ningbo SCIENTZ Biotechnology Co., Ltd., China) with the 100 W power of ultrasonic wave. Prior to SEM observation, the samples were sputtering-coated with a thin layer of Pt/Pd alloy to enhance the conductivity.

Results and discussion

TG analysis. TG plot is displayed in Figure 1, where a gradual losing weight appears between 20 and 165 °C, and the whole weight loss is estimated to be ca. 5.1% and this value is in agreement with that losing one H_2O together with one MeOH per formula unit $[Fe(NH_2\text{-}Trz)_3](doe)_2 \cdot H_2O \cdot MeOH$ (calculated to be 5.8%), this result is also consistent with that obtained from elemental analysis as well as TGA-Mass experiment for **1** (see Figure S2 and S3).

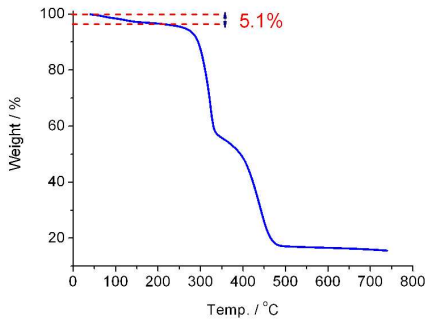

Figure 1 TG plot of **1** between 20 an 750 °C.

Magnetic susceptibility and DSC. Temperature dependent magnetic susceptibility of **1** is shown in Figure 2 in both forms of χ_m–T and χ_mT–T, where χ_m represents the molar magnetic susceptibility of **1** with one Fe^{2+} ion per formula unit. A magnetic transition between high-spin and low-spin states, with ca. 13 K hysteresis loop, appears in the temperature interval 305–325 K and the Curie-Weiss-type magnetic susceptibility occurs below 250 K (Figure 2a), which arises from the magnetic impurity related to the lattice defects. The equation (1) is used to estimate the magnetic susceptibility contributed from the paramagnetic impurity, atom core diamagnetism and possible van Vleck paramagnetism,

$$\chi_m = \frac{C}{T-\theta} + \chi_0 \qquad (1)$$

Where the first term represents the paramagnetic susceptibility contributed from magnetic impurity, and the χ_0 includes the diamagnetic susceptibility contributed from atom core in molecule and possible temperature-independent van Vleck paramagnetic susceptibility related to the coupling of the ground and excited states through a magnetic field.[38] The best fitting for the χ_m-T plot in the temperature ranges 1.8-250 K yielded the parameters of C = 1.58(16)×10^{-1} emu·K·mol^{-1}, θ = -1.69(5) K and χ_0 = 3.3(4)×10^{-4} emu·mol^{-1} with the correlation coefficient R^2 = 0.999. From the fitted Curie constant, a fraction of ~5% of S = 2 magnetic impurities is estimated if g = 2.0 was assumed. On the basis of the fit, the molar magnetic susceptibility contributed from 1-D Fe^{2+} coordination polymer chain was obtained via removing the terms of C/(T-θ) and χ_0, and the corrected magnetic susceptibility in χ_mT form as a function of temperature was given in Figure 2b and the corresponding d(χ_mT)/dT *versus* T plot was displayed in the inset of Figure 2b where two peaks appeared respectively at 309.8 and 322.8 K with ΔT_{Peak} = 13 K. The χ_mT value was estimated to be ca. 2.8 emu·mol^{-1} at 400 K, from Figure 2b, and slight smaller than the theoretical value 3.0 emu·mol^{-1} (with g = 2.0) of one molar Fe^{2+} ion in high-spin (HS) state; the χ_mT product is close to zero below 250 K, indicating that a complete spin transition between HS and LS states undergoes in **1**. This situation is somewhat distinct from the findings by Létard and coworkers who examined the consequence of particle size reduction on the thermal and light-induced magnetic properties of the SCO coordination polymer $[Fe(NCS)_2(bpe)_2]\cdot n$(solvent) where bpe = 1, 2-bis(4'-pyridyl)ethane, and found that the retention of the HS state increases with reducing the particle size.[30]

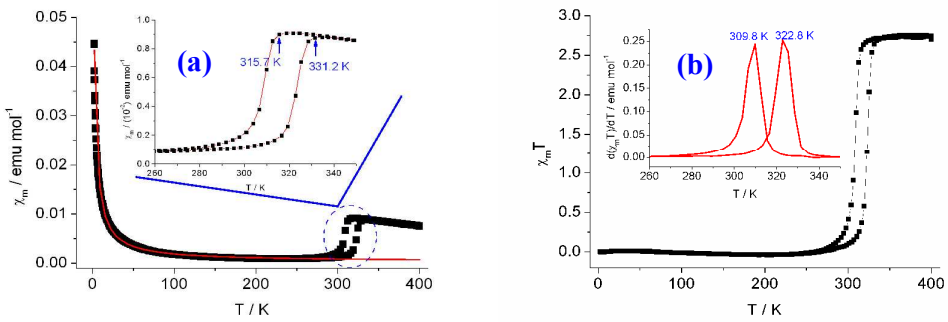

Figure 2 Temperature dependence of magnetic susceptibility in the form of (a) χ_m–T where the black squares represent the experimental data and red line was theoretically reproduced using the fitted parameters (ref. the main text) (b) χ_mT–T for **1** in a cooling-heating cycle (Inset: Derivative of χ_mT with respect to T in cooling and heating modes).

DSC curves are shown in Figure 3, in which a reversible thermal anomaly appears. The thermal anomaly temperature obtained from magnetic susceptibility and DSC measurements show a little bit difference owing to the rate of temperature change is distinct between two measurement techniques and the analogous situation was also observed in other spin-crossover systems.[39, 40] The ΔH and ΔS (ΔS = ΔH/T_C) are estimated to be 24.3 kJ·mol^{-1} and 75.0 J·K^{-1}·mol^{-1} for the thermal anomaly in heating run. For the spin transition between S = 2 HS state and S = 0 LS state, the spin entropy difference is theoretically equal to $R\ln(2S_{HS}+1)/(2S_{LS+1}) \approx 13.4$ J·K^{-1}·mol^{-1} (where R is the gas constant, S_{HS} and S_{LS} represent the spin values in high-spin and low-spin states, respectively). These results revealed that the dominant part (ca. 80%) of the entropy change arises from contributions of inter- and intramolecular vibrations, which therefore are the major driving force for the spin crossover process. The remaining ca. 20 % of ΔS is the electronic (magnetic) contribution of the spin change. The situation that the inter- and intramolecular vibrations dominate the entropy change between spin state transformations was also found in $[Fe(phen)_2(NCS)_2]$ spin-crossover system.[41]

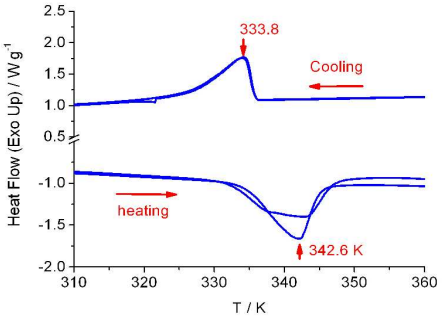

Figure 3 DSC traces of **1** in two sequential thermal cycles at a heating/cooling rate of 10 K·min^{-1}.

Raman spectra. Raman spectra of **1** at selected temperatures are shown in Figure 4. There is absent change associated with the spin transition for most of vibration bands in variable-temperature Raman spectra of **1**. For instance, there are five Raman bands in the ranges of 2700 and 3000 cm^{-1}, corresponding to the stretching vibrations of C-H in $-CH_2-$ and $-CH_3$ moieties of alkyl chain as well as their Fermi resonance.[42]

The bands in the regions of 1325–1525 cm^{-1}, 980–1000 cm^{-1}, 400–460 cm^{-1} and 230–270 cm^{-1} are found to change with the spin transition. The band centered at 1375 cm^{-1} has two shoulders at both sides of the main peak, which arise from the vibration models of $\omega(CH_2)$[42] or $\nu(C–NNH_2)$,[33] and the intensities of two shoulders increase with increasing temperature respect to the main peak. Three bands located at 1440, 1450 and 1484 cm^{-1} at room temperature and assigned to $\gamma(CH_2)$,[42] ν(C–N) and $\nu(C–NNH_2)$[33] combine to form an asymmetric band when temperature is above 36 °C. As show in Figure 4c and 4d, the band centered at 1027 cm^{-1} in low-spin state, attributed to ν(C–N) or δ(ring)[33] of 4-amino-1, 2, 4-triazole ligands, shifts toward high frequency, while the band located at 437 cm^{-1}, assigned to $\delta(C–N–NH_2)$[33] of 4-amino-1, 2, 4-triazole, moves to low frequency with spin state change. Two bands near 250 cm^{-1} which arise from the stretching vibration of ν(Fe-N) appear in low-spin state,[30] whereas vanish in high-spin state. It is worth noting that the changes of these bands occur around 36–45 °C upon heating and this temperature is close to the transition temperature observed from magnetic susceptibility measurement in the heating model.

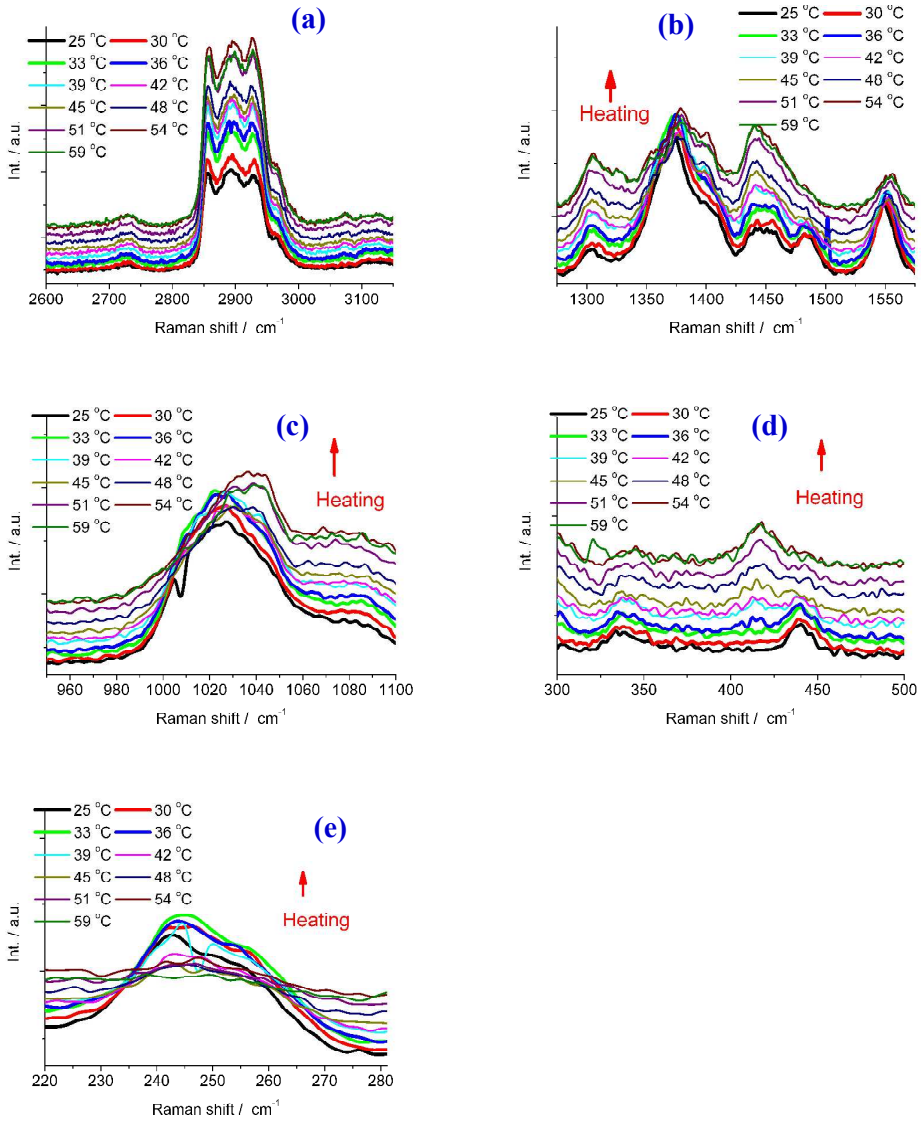

Figure 4 Raman spectra of a powder sample of **1** at selected temperatures upon heating in the ranges (a) 2600-3150 cm^{-1} (b) 1250-1600 cm^{-1} (c) 950-1100 cm^{-1} (d) 300-500 cm^{-1} (e) 220-280 cm^{-1}.

SEM photograph of nanoparticles and optical picture of transparent disc. Figure 5a shows SEM photo of nanoparticles of **1**. The monodisperse spherical particles, aggregated from sheet-shaped nanocrystals, have dimensions of 200–300 nm and the particle size distribution is displayed in Figure 5b. We investigated the influence of the reaction parameters, such as reaction time, temperature and the molar ratios of reactants, on the particle sizes of **1**, and found that the particle sizes of **1** are

not significantly affected by the above-mentioned reaction parameters, whereas remarkably related to the power of ultrasonic wave for distribution of particles. As shown in Figure S5, the particle sizes of **1** become obviously smaller when the power of ultrasonic wave was applied from 100 W to 200 W. This is understandable because the particles are aggregated from sheet-shaped nanocrystals which are bound to each other via van der Waals forces and easily separated under high power of ultrasonic wave.

Interestingly, the nanoparticles of **1** were pressed under ca. 8 MPa static pressure to give optically transparent disc. As shown in Figure 5c and 5d, such a disc with a thickness of ca. 1.0 mm is pink-violet color at room temperature, which is due to the $^1A_1$ to $^1T_1$ d-d transition of Fe^{2+} ions in the LS state (the corresponding UV-visible spectrum is displayed in Figure 5e), and transparent so that the letter "A" written on the aluminum foil under the disc can be visibly seen. The disc color changes obviously from pink-violet in LS state to yellowish in HS state accompanied with the spin transition (the color of **1** in HS state is due to the $^5T_2$ to ^5E d-d transition of Fe^{2+} ions in the HS state), and the letter "A" on the aluminum foil becomes more clear.

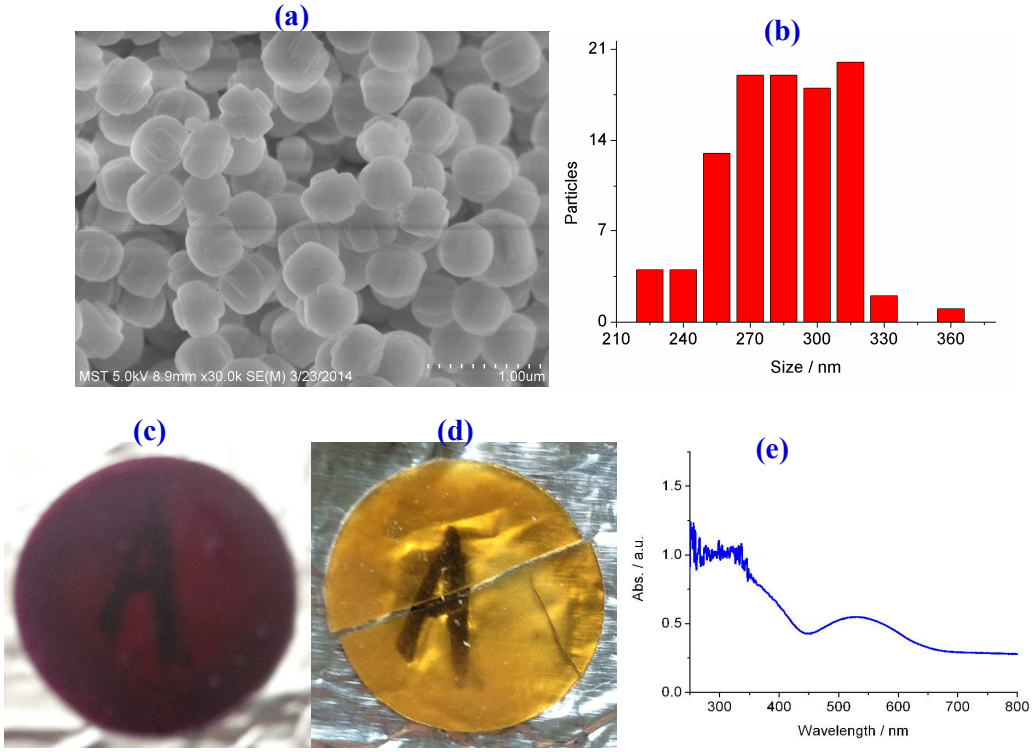

Figure 5 (a) SEM photograph showing monodisperse nanoparticles of **1** (b) distribution of particle sizes and optical images for a transparent disc in (c) LS (d) HS states which display distinct colors (e) UV-visible spectrum in solid state at ambient temperature (LS state, and the maximum around 530 nm is attributed to $^1A_1$ to $^1T_1$ d-d transition of Fe^{2+} ions in the LS state).

Conclusion

In summary, we fabricated monodisperse nanoparticles of a one-dimensional spin-crossover polymer using a facile precipitation approach. The nanoparticles aggregate from plate-shaped nanocrystals and their size dimensions fall in the ranges of 200–300 nm. The spin-crossover polymer undergoes a thermal reversible spin transition, with ca. 13 K hysteretic loops, near room temperature. The spin-crossover polymer nanoparticles were pressed under the ca. 8 MPa static pressure to give a good transparent disc with a thickness of ca. 1 mm, such a disc shows pink-violet color at ambient temperature while yellowish color above 45 °C. This spin-crossover material has potential applications in the field of thermochromic devices such as thermometers (fever indicators, gadgets, design applications, etc.) or warning signals (e.g., on heaters).

Acknowledgement

Authors thank the Priority Academic Program Development of Jiangsu Higher Education Institutions, Science and National Nature Science Foundation of China for financial support (grant nos. 91122011 and 21271103).

Notes and References

1. O. Kahn, C. J. Martinez, *Science*, 1998, **279**, 44.
2. T. Liu, D. P. Dong, S. Kanegawa, S. Kang, O. Sato, Y. Shiota, K. Yoshizawa, S. Hayami, S. Wu, C. He, C. Y. Duan, *Angew. Chem. Int. Ed.*, 2012, **51**, 4367.
3. S. Takaishi, N. Ishihara, K. Kubo, K. Katoh, B. K. Breedlove, H. Miyasaka, M. Yamashita, *Inorg. Chem.*, 2011, **50**, 6405.
4. M. Nihei, H. Tahira, N. Takahashi, Y. Otake, Y. Yamamura, K. Saito, H. Oshio, *J. Am. Chem. Soc.*, 2010, **132**, 3553.
5. F. Setifi, S. Benmansour, M. Marchivie, G. Dupouy, S. Triki, J. Sala-Pala, J.-Y. Salaün, C. J. Gómez-García, S. Pillet, C. Lecomte, E. Ruiz, *Inorg. Chem.*, 2009, **48**, 1269.
6. O. Jeannin, R. Clérac, M. Fourmigué, *J. Am. Chem. Soc.* 2006, **128**, 14649.
7. W. Fujita, K. Awaga, *Science*, 1999, **286**, 261.
8. M. E. Itkis, X. Chi, A. W. Cordes, R. C. Haddon, *Science*, 2002, **296**, 1443.
9. J. A. Koza, Z. He, A. S. Miller, J. A. Switzer, *Chem. Mater.*, 2011, **23**, 4105.
10. C. Z. Wu, J. Dai, X. D. Zhang, J. L. Yang, Y. Xie, *J. Am. Chem. Soc.*, 2009, **131**, 7218.
11. Y. Muraoka, Z. Hiroi, *Appl. Phys. Lett.*, 2002, **80**, 583.
12. E. König. G. Ritter, S. K. Kulshreshtha, *Chem. Rev.*, 1985, **85**, 219.
13. J. A. Real, A. B. Gaspar, V. Niel, M. C. Muñoz, *Coord. Chem. Rev.*, 2003, **236,** 121.
14. R. Boca, W. Linert, *Monatsh. Chem.*, 2003, **134,** 199.
15. D. S. Middlemiss, D. Portinari, C. P. Grey, C. A. Morrison, C. C. Wilson, *Phys. Rev. B*, 2010, **81**, 184410.
16. D. Papanikolaou, W. Kosaka, S. Margadonna, H. Kagi, S. Ohkoshi, and K. Prassides, *J. Phys. Chem. C*, 2007, **111**, 8086.
17. A. Bousseksou, F. Varret, M. Goiran, K. Boukheddaden and J.-P. Tuchagues, *Top. Curr. Chem.,* 2004, **235**, 65.
18. P. Gütlich, Y. Garcia, T. Woike, *Coord. Chem. Rev.*, 2001, **219–221,** 839.
19. J.-F. Létard, P. Guionneau, L. Goux-Capes, *Top. Curr. Chem.*, 2004, **235,** 221.

20. A. Bousseksou, G. Molnar, L. Salmon, W. Nicolazzi, *Chem. Soc. Rev.*, 2011, **40,** 3313.
21. A. Carné, C. Carbonell, I. Imaz, D. Maspoch, *Chem. Soc. Rev.*, 2011, **40,** 291.
22. G. Gallé, D. Deldicque, J. Degert, T. Forestier, J.-F. Létard and E. Freysz, *Appl. Phys. Lett.*, 2010, **96,** 041907.
23. C. Barraud, P. Seneor, R. Mattana, S. Fusil, K. Bouzehouane, C. Deranlot, P. Graziosi, L. Hueso, I. Bergenti, V. Dediu, F. Petroff, A. Fert, *Nat. Phys.*, 2010, **6**, 615.
24. Z. H. Xiong, D. Wu, Z. V. Vardeny, J. Shi, *Nature*, 2004, **427**, 821.
25. E. Coronado, J. R. Galán-Mascarós, M. Monrabal-Capilla, J. García-Martinez, P. Pardo-Ibáñez, Adv. Mater. 2007, 19, 1359.
26. T. Forestier, S. Mornet, N. Daro, T. Nishihara, S.-I. Mouri, K. Tanaka, O. Fouché, E. Freysz, J.-F. Létard, Chem. Commun. 2008, 4327.
27. F. Volatron, L. Catala, E. Rivière, A. Gloter, O. Stéphan, T. Mallah, Inorg. Chem. 2008, 47, 6584; I. Boldog, A. B. Gaspar, V. Martínez, P. Pardo-Ibañez, V. Ksenofontov, A. Bhattacharjee, P. Gütlich, J. A. Real, Angew. Chem. Int. Ed. 2008, 47, 6433.
28. J. Larionova, L. Salmon, Y. Guari, A. Tokarev, K. Molvinger, G. Molnár, A. Bousseksou, Angew. Chem. Int. Ed. 2008, 47, 8236.
29. T. Forestier, A. Kaiba, S. Pechev, P. Guionneau, N. Daro, E. Freysz, J.-F. Létard, Chem. Eur. J. 2009, 15, 6122.
30. S. M. Neville, C. Etrillard, S. Asthana, J.-F. Létard, *Eur. J. Inorg. Chem.* 2010, 282.
31. O. Fouche, J. Degert, G. Jonusauskas, N. Daro, J.-F. Létard and E. Freysz, *Phys. Chem. Chem. Phys.*, 2010, **12,** 3044.
32. M. M. Dîrtu, A. Rotaru, D. Gillard, J. Linares, E. Codjovi, B. Tinant and Y. Garcia, *Inorg. Chem.*, 2009, **48**, 7838.
33. S. Rackwitz, J. A. Wolny, K. Muffler, K. Achterhold, R. Rüffer, Y. Garcia, R. Diller and V. Schünemann, *Phys. Chem. Chem. Phys.*, 2012, **14**, 14650.
34. A. Grosjean, N. Daro, B. Kauffmann, A. Kaiba, J.-F. Létard and P. Guionneau,

Chem. Commun., 2011, **47**, 12382.

35. Y. A. Tobon, L. Kabalan, S. Bonhommeau, N. Daro, A. Grosjean, P. Guionneau, S. Matar, J.-F. Létard, F. Guillaume, *Phys. Chem. Chem. Phys.*, 2013, **15**, 18128.
36. A. Tokarev, L. Salmon, Y. Guari, G. Molnár, A. Bousseksou, *New J. Chem.,* 2011, **35**, 2081.
37. J. G. Haasnoot, *Coord. Chem. Rev.*, 2000, **200**, 131.
38. J.H. van Vleck, The Theory of Electric and Magnetic Susceptibilities, Oxford, London, 1932.
39. R. Kulmaczewski, J. Olguín, J. A. Kitchen, H. L. C. Feltham, G. N. L. Jameson, J. L. Tallon, S. Brooker, *J. Am. Chem. Soc.*, 2014, **136**, 878.
40. F. Volatron, L. Catala, E. Rivière, A. Gloter, O. Stéphan, T. Mallah, *Inorg. Chem.*, 2008, **47**, 6584.
41. M. Sorai and S. Seki, *J. Phys. Chem. Solids*, 1974, **35**, 555.
42. M. Picquart. *J. Phys. Chem.*, 1986, **90**, 243.